Optimizing the Performance of a New Current Source Type Grid-Forming Modular Multilevel Converter Using Genetic Algorithms

Chen Jiang, Jhair S. Acosta, and Aniruddha M. Gole
Department of Electrical and Computer Engineering, University of Manitoba, Winnipeg, Canada
jiangc38@myumanitoba.ca, {jhair.acostasarmiento1, Aniruddha.Gole}@umanitoba.ca

***Abstract*—Modular Multilevel Converters (MMC) have found extensive application in connecting Renewable Energy Sources to the power grid. Recently, MMCs operated in the Grid Forming (GFM) mode have garnered significant interest due to their superior performance in weak AC networks. The Virtual Synchronous Generator (VSG) is a GFM technology designed to emulate the behavior of a real synchronous generator (SG). There is flexibility in selecting the VSGs parameters as they are not constrained by the physical attributes of an actual SG. This paper proposes employing the Genetic Algorithm (GA) to select these parameters, underscoring its simplicity and effectiveness in meeting diverse constraints and objectives. Small Signal (SS) models are constructed at potential operational points, with GA leveraging the SS model's eigenvalues to select parameter values that enhance dynamic performance, ensuring resilience across a wide range of operating conditions. The effectiveness of these designed parameters is validated through Electromagnetic Transients (EMT) simulations.**

***Index Terms*—Electromagnetic Transients (EMT) Simulation, Grid-forming (GFM) Converter, Genetic Algorithm (GA), Modular Multilevel Converter (MMC), Virtual Synchronous Generator (VSG).**

I. Introduction

With increasing concern in climate change and energy shortages, there is a rising trend of incorporating renewable energy sources (RES) into the power grid. Generally, these resources have poor power quality and the generated voltage is usually not at the $50\ Hz$ or $60\ Hz$ grid frequency. Hence, Voltage Source Converters (VSCs) have become the dominant means of connecting these resources to the grid [1]. They condition the RES output to grid quality. Typically, the VSC control mode can be classified as grid-following (GFL) and grid-forming (GFM). The GFL mode requires a phase-locked loop (PLL) to track the phase of the system voltages and generate the on/off firing signals for the VSCs switches. However, the tracking capability becomes compromised when there is a high penetration of RES in the network [2]. Alternatively, the GFM converter generates its own output voltage whose magnitude and phase are adjusted to meet the desired active and reactive powers. It does not require an external phase synchronization element such as the PLL.

The virtual synchronous generator (VSG) is one possible GFM strategy, in which the converter mimics the characteristics of a synchronous generator (SG). In most earlier work on the conventional VSG, only the electro-mechanical swing equation is used to generate the magnitude and phase of the VSGs output [3]. This model does not include the full electrical representation of a real SG, but is easy to implement and correctly reproduces the low frequency electro-mechanical behaviour. It can be improved by incorporating additional blocks such as an extra damping loop [4], virtual impedance controller [5] [6] and so on. One problem with a conventional VSG is that its power-electronic switches cannot handle the fault currents of a real SG, and so a current limiting control feature has to be added. This current limiter uses a decoupled current controller and limits the current references in order to avoid overcurrent. It generates a voltage order for the VSC by passing the error between current orders and actual currents through Proportional-Integral (PI) controllers. However, [7] shows that the VSG can become unstable due to the additional delays introduced by these PI controllers, when connected to a strong ac system.

Recently, a new VSG control method has been proposed for the Modular Multilevel Converters (MMC), where it can be operated as a stiff current source [8]. This removes the requirement for having a PI controller in the current limiter because the current order itself can be limited. It also allows the representation of a more accurate model of the synchronous generator. Research has shown that the losses of the current-controlled VSG are similar to that a voltage controlled VSG [9]. Moreover, [10] indicates that this current source interfaced VSG can provide stable operation in both very weak and very strong ac systems. The proposed VSG has several user-settable parameters, e.g., inertia constant, damping constant, different (virtual) stator, field and damper winding inductances and resistances in the d and q axes, etc. These can be freely chosen, as there is no requirement they must fall in typical parameter range of a real machine. However, the wide choice also makes it difficult to find an optimum parameter set. An option used earlier started with using datasheet parameters of an actual SG, and then manually adjusting these by trial and error to improve the response. However, this approach does not explore a very wide range of parameters and is also time consuming.

In contrast, this paper exploits a non-linear optimization approach to determine multiple parameter values that result in a good dynamic response. The parameters are selected

using a Genetic Algorithm (GA) with the objective function ensuring that the damping ratio of the most dominant mode is essentially $1/\sqrt{2}$ [11]. This results in the system attaining the desired operating condition with reasonable speed and without excessive oscillations and large overshoots.

From a broad perspective, optimization techniques found in literature can be classified into classical and heuristic techniques. Classical optimization uses derivatives of various orders or equivalent methods to determine the direction of steepest descent for the objective function (OF). The next trial point in the decision variable space is then selected along this direction with a view to minimizing the OF. This implies that the problem must be formulated in a manner where the OF depends on the decision variable derivatives. However, in many real problems, it is not possible to meet this condition. Sometimes, the function is not differentiable or continuous; and often deriving a mathematical formulation may be too complex or the model may be provided as a "black" or "grey" box by a third party. In such cases, numerical simulation has to be used to obtain the OF values. Also, the search space may be extremely large as with combinatorial problems. In such cases, heuristic techniques come in handy [12].

The most popular heuristics techniques nowadays are inspired by nature [13] and include evolutionary algorithms such as Genetic Algorithms (GAs) which have been used to optimize a wide variety of problems in several fields. They typically use the concepts of genetics, evolution, and natural selection [14]. GAs are very popular because they are simple to code, and have demonstrated ability to solve complex and multi-modal problems in reasonable times, while performing a local and global search in a very large decision space.

The optimization problem presented in this paper involves a complex non-linear mathematical model. Therefore, GAs are a suitable option as the optimization algorithm. In this sense, GAs are selected in this paper, considering that they are simple, effective and highly customizable, allowing for the incorporation of different constraints and objectives [15]. However, any other optimization algorithm capable of solving non-linear with many variables could have been selected. Some possible options include Particle Swarm Optimization (PSO), Differential Evolution (DE), Ant Colony, etc. Classical optimization methods can often locate only a local optimum. GAs on the otherwise are known to converge to the global optimum if there is no restriction on the number of iterations, which is never the case. Nevertheless, GA still give a high quality optimized result [16].

The aim of the optimization is to carefully select the parameters of a VSG to attain a well-damped behavior. It would be possible to derive the objective function by conducting Electromagnetic Transients (EMT) simulation [17], but that would be extremely time consuming. As an alternative, a small signal (SS) model is constructed, and the objective function is derived by inspecting its eigenvalues [18]. GA optimization is performed directly on the eigenvalues to select the optimal parameters. Finally EMT simulation is used to validate the optimized results.

II. Current Source Interfaced Virtual Synchronous Generator and its Small Signal Model

This section introduces the current source interfaced VSG and its small signal model.

A. Overall VSG Structure

The structure of the current source interfaced VSG is shown in Fig. 1. The overall VSG model has the following sub-parts: i) Mechanical Equations, ii) Electrical Equations and iii) Excitation System. The mechanical and electrical parts exchange torque (T_m, T_e) as well as speed (ω) information and finally generate the phase current references $i_{ref}^{abc} = [i_{ref}^{a}, i_{ref}^{b}, i_{ref}^{c}]$. A current magnitude limiting block is incorporated to limit these references to a safe value so as not to damage the semiconductor switches of the VSG converter. The mechanical model includes the swing equation of the machine [18] and outputs the virtual rotor angle θ (analog of the actual rotor angle in a SG). The generated angle θ is used in dq/abc transformation (Parks transformation) for converting to/from phase and dq-axis quantities. Additionally, the excitation system operates on the voltage difference (error) between the terminal voltage V and its reference V_{ref}, and outputs the field voltage E_{fd} with a view to minimizing this error.

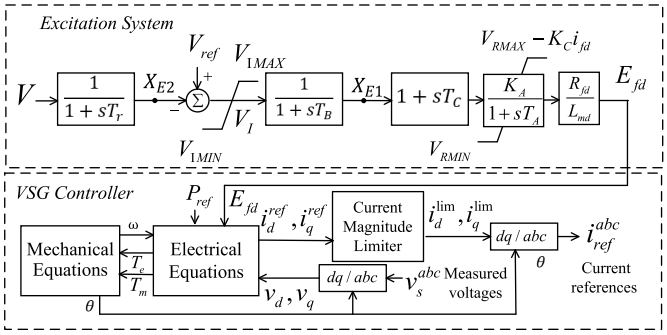

Fig. 1. Overall controller structure.

B. Mechanical System and Electrical Equations

The VSGs parameters are summarized in Table I.

TABLE I
Parameters of the VSG

Parameter	Explanation
H	Inertia constant
D_w	Damping constant
R_a	Virtual stator resistance
R_{1d}	Virtual damper resistance in d-axis
R_{fd}	Virtual field winding resistance
R_{1q}	Virtual damper resistance in q-axis
L_a	Virtual leakage inductance
L_{md}	Virtual mutual inductance in d-axis
L_{fd}	Virtual field winding inductance
L_{1d}	Virtual damper inductance in d-axis
L_{mq}	Virtual mutual inductance in q-axis
L_{1q}	Virtual damper inductance in q-axis

1) Mechanical Equations: The mechanical model uses the core swing equation of the SG as shown in (1) [18]. It computes and outputs the VSGs virtual angular speed ω and virtual rotor angle θ based on the mechanical (T_m) and electromagnetic (T_e) torques. Also, P_{ref} is the active power reference and ω_0 is the nominal angular frequency of the grid.

$$\begin{cases} 2H\frac{d\omega}{dt} = T_m - T_e - D_w\omega \\ \frac{d\theta}{dt} = \omega \\ T_m = \frac{P_{ref}}{\omega} + D_w\omega_0 \end{cases} \tag{1}$$

2) Electrical Equations: The d- and q-axis equivalent circuits of the VSG are given in Fig. 2 and have exactly the same form as those of a real SG [18]. The d and q components of terminal voltage are v_d, v_q. The d-axis has a field winding and one damper winding; and the q-axis has one damper winding. The currents i_d, i_{fd}, i_{1d}, are the d-axis stator, field and damper winding currents, and i_q, i_{1q} are the q-axis stator and damper currents. The corresponding flux linkages are ψ_{fd}, ψ_{1d}, etc. For brevity, p represents the time derivative operator e.g., $p\psi_d = d\psi_d/dt$.

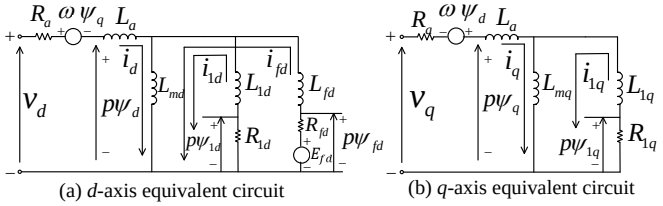

(a) *d*-axis equivalent circuit (b) *q*-axis equivalent circuit

Fig. 2. Electrical equivalent circuits of the VSG.

From Fig. 2, the equations for the VSG can be stated as in (2)-(11). Using these equations, the flux linkages can be calculated by a suitable numerical integration method (e.g., RK-2 method, trapezoidal rule, etc.), and then the currents are determined using (2)-(6). In this paper, a current controlled MMC would be used to inject these currents into the network, but is not discussed further, because it is not germane to the development of the small signal equations used in the optimization process. It is however, included in the full EMT simulation used for validation.

$$\psi_d = (L_a + L_{md})i_d + L_{md}i_{1d} + L_{md}i_{fd} \tag{2}$$

$$\psi_{1d} = L_{md}i_d + (L_{1d} + L_{md})i_{1d} + L_{md}i_{fd} \tag{3}$$

$$\psi_{fd} = L_{md}i_d + L_{md}i_{1d} + (L_{fd} + L_{md})i_{fd} \tag{4}$$

$$\psi_q = (L_a + L_{mq})i_q + L_{mq}i_{1q} \tag{5}$$

$$\psi_{1q} = L_{mq}i_q + (L_{mq} + L_{1q})i_{1q} \tag{6}$$

$$\frac{d\psi_d}{dt} = v_d - i_dR_a - \omega\psi_q \tag{7}$$

$$\frac{d\psi_{1d}}{dt} = -R_{1d}i_{1d} \tag{8}$$

$$\frac{d\psi_{fd}}{dt} = E_{fd} - R_{fd}i_{fd} \tag{9}$$

$$\frac{d\psi_q}{dt} = v_q + \omega\psi_d - R_ai_q \tag{10}$$

$$\frac{d\psi_{1q}}{dt} = -R_{1q}i_{1q} \tag{11}$$

Also, the electrical torque T_e required in (1) is calculated as in (12).

$$T_e = \psi_di_q - \psi_qi_d \tag{12}$$

C. Small Signal Model of Proposed VSG

Equations (1)-(12) and also the excitation system equations shown in Fig. 1 are linearized at a steady state operating point, from which the small signal (SS) model given by (13) is developed. Its eigenvalues define the stability and dynamic behaviour. The exact form and derivation of the matrices $\boldsymbol{A}$ and $\boldsymbol{B}$ are described in detail in [10], which is not shown here due to page limitations.

$$\frac{d\boldsymbol{\Delta x}}{dt} = \boldsymbol{A}\boldsymbol{\Delta x} + \boldsymbol{B}\boldsymbol{\Delta u} \tag{13}$$

In (13), the $\boldsymbol{\Delta u}$ are the inputs to the model and $\boldsymbol{\Delta x}$ are the state variables as defined in (14) and (15).

$$\boldsymbol{\Delta x} = (\Delta\psi_d, \Delta\psi_{1d}, \Delta\psi_{fd}, \Delta\psi_q, \Delta\psi_{1q}, ... \\ ...\Delta\omega, \Delta\delta, \Delta E_{fd}, \Delta X_{E1}, \Delta X_{E2})^T \tag{14}$$

$$\boldsymbol{\Delta u} = (\Delta P_{ref}, \Delta V_{ref})^T \tag{15}$$

D. Eigenvalue Analysis

According to the Lyapunov's first method, the small signal stability of a non-linear system can be determined from the eigenvalues of its linearized SS model matrix $\boldsymbol{A}$ [19]. The general format of the k^{th} eigenvalue is expressed in (16).

$$\lambda_k = \sigma_k + j\omega_k \tag{16}$$

If all the eigenvalues are in the left-hand plane, i.e., $\sigma < 0$, the system is stable. The damping ratio ξ_k which is used to describe the velocity of attenuation can be calculated as given in (17). With a larger damping ratio, the system has a better performance with a shorter settling time. Therefore, ξ_k is used to quantify the response quality in the optimization process, which attempts to make ξ_k move closer the optimal value of 0.707 [11]. Additionally, the oscillation frequency is calculated as $f_{nk} = \omega_k/2\pi$.

$$\xi_k = \frac{-\sigma_k}{\sqrt{\sigma_k^2 + \omega_k^2}} \tag{17}$$

III. Optimization Method: Genetic Algorithm

A. Optimization Process

The optimization procedure requires the definition of a fitness function to be maximized. The GA method works with a population $\mathbf{P_o} = \{\vec{S}_1, \vec{S}_2, ..., \vec{S}_N\}$, comprised of N individual sets referred to as "solutions". Each solution is a vector composed of the real decision variables that influences the damping ratio in the SS model, i.e., $\vec{S}_n = [H, D, R_a, R_{fd}, R_{kd}, R_{1q}, L_a, L_{md}, L_{fd}, L_{kd}, L_{mq}, L_{1q}]$.

Let $\mathbf{P_{o_1}}$ be the initial population at generation 1. Starting with this, subsequent generations of populations $\mathbf{P_{o_g}}$, with

$g = 1, 2, \cdots, G$, are evolved during G generations with the aim of improving the fitness of the solutions, using an analogy with a biological evolutionary process. At each generation, the GA creates an "offspring" population $\mathbf{Q_{o_g}}$ by operating on the individuals in $\mathbf{P_{o_g}}$, using the arithmetic crossover presented in Algorithm 1 below. Then, random mutations are applied to the individuals in $\mathbf{Q_{o_g}}$ by following Algorithm 2.

Algorithm 1 Arithmetic crossover

$\mathbf{Q_{o_g}} \leftarrow$ empty
while $size(\mathbf{Q_{o_g}}) < N$ **do**
  From $\mathbf{P_{o_g}}$ select two random progenitors $\vec{p1}_d$ and $\vec{p2}_d$
  $\alpha_0 \leftarrow$ random number $\in$ [0,1]
  if $\alpha_0 \leq$ crossover probability **then**
    for $d = 1$, $d \leq size(\vec{p1}_d)$, $d++$ **do**
      $\alpha \leftarrow$ random number $\in$ [0,1]
      $q1_d \leftarrow \alpha p1_d + (1-\alpha)p2_d$
      $q2_d \leftarrow \alpha p2_d + (1-\alpha)p1_d$
    Add $\vec{p1}$ to $\mathbf{Q_{o_g}}$
    if $size(\mathbf{Q_{o_g}}) < N$ **then**
      add $\vec{p2}$ to $\mathbf{Q_{o_g}}$

Algorithm 2 Mutation

let $\vec{q}$ be the vector of decision variables of a particular offspring.
let $\mathcal{N}(0,1)$ be a gaussian distribution with mean 0 standard deviation of 1,
for $d = 1$, $d \leq size(\vec{q})$, $d++$ **do**
  $\alpha \leftarrow$ random number $\in$ [0,1]
  if $\alpha \leq$ mutation probability **then**
    $q_d \leftarrow q_d + 0.1\mathcal{N}(0,1)$

After that, the offspring and parent populations are combined ($\mathbf{P_{o_g}} \leftarrow \mathbf{P_{o_g}} \cup \mathbf{Q_{o_g}}$) into a single population with $2N$ individuals. At the end of each generation, using the "modified tournament" in Algorithm 3, N individuals are eliminated to create the population of the next generation ($\mathbf{P_{o_{g+1}}}$), which once again has N individuals.

Algorithm 3 Modified Tournament

for each individual $\vec{S}_n$ in $\mathbf{P_{o_g}}$ **do**
  $\vec{S}_{n_{score}} = 0$
  $\mathbf{P_t} \leftarrow 0.2N$ random individuals form $\mathbf{P_{o_g}}$
  for each individual $\vec{S}_{n_2}$ in $\mathbf{P_t}$ **do**
    if fitness($\vec{S}_{n_2}$) < fitness($\vec{S}_n$) **then**
      $\vec{S}_{n_{score}} = \vec{S}_{n_{score}} + 1$
$\mathbf{P_{o_g}} \leftarrow N$ individuals with highest $\vec{S}_{n_{score}}$

This simplified explanation was given to show the basic process. In the actual implementation, at the beginning of each generation, the original population $\mathbf{P_{o_g}}$ is augmented with $N/10$ randomly generated individuals to increase the population diversity, helping to explore the solution space in a better way.

B. Fitness Function and Constraint Handling

The fitness function given in (18) ensures that the damping ratio of the dominant eigenvalue ξ_{dom} is made as close as possible to the optimal value of $\xi_{opt} = 1/\sqrt{2}$; subject to all decision variables being positive (i.e., $\{H, D, R_a, R_{fd}, R_{kd}, R_{1q}, L_a, L_{md}, L_{fd}, L_{kd}, L_{mq}, L_{1q}\} > 0$); and all eigenvalue being stable ($\sigma_k < 0$). The above objectives are coded into the fitness function (18), which includes the penalty function to ensure the constraints. The first part in (18) helps to maximize the smallest damping ratio for any of the K eigenvalues ($\lambda_k = \sigma_k + j\omega_k$), while the second part uses a penalty function P (20) to penalize the solutions that do not meet the constraints defined. This helps to create promissory solutions from those that do not satisfy the constraints.

$$fitness(\vec{S}_n) = \xi_{dom} + P \tag{18}$$

where:

$$\xi_{dom} = \min\left(\frac{-\sigma_k}{\sqrt{\sigma_k^2 + \omega_k^2}}\right) \tag{19}$$

with:

$$\begin{aligned} P = &-\frac{|\xi_{dom} - \xi_{opt}|}{\xi_{opt}}, \text{ if } \xi_{dom} > \xi_{opt} \\ &- \sum_{k=1}^{K} |\sigma_k|, \text{ if } \sigma_k < 0 \\ &- \sum_{d=1}^{size(\vec{S}_n)} 100|\vec{S}_{n,d}|, \text{ if } \vec{S}_{n,d} < 0 \end{aligned} \tag{20}$$

IV. Example System

The example system consists of an MMC with 200 submodules (SMs) per arm as shown in Fig. 3 and operated as a current source interfaced VSG [9]. It is connected to an ac network with a short circuit ratio (SCR) of 4.5. The main system parameters are in Table II.

From Fig. 3, the outputs of the VSG are the current references i_{ref}^{abc}. Then i_{ref}^{abc} is transferred to the hysteresis current controller to generates the required voltage references v_{ref}^{abc} so that the MMC currents i^{abc} are essentially equal to i_{ref}^{abc}. A novel hysteresis current controller using acceleration current slope is used in this case to control the MMC as a high-bandwidth and high-precision current source to generate any desired current waveforms [9]. This method generates the instantaneous three phase voltage references v_{ref}^{abc} for the MMC, which makes use of the multiple voltage steps available with the MMC and accelerates or decelerates the rate of change of current depending on whether it deviates significantly from the target current. Therefore, the output current is confined to a narrow envelope around its reference.

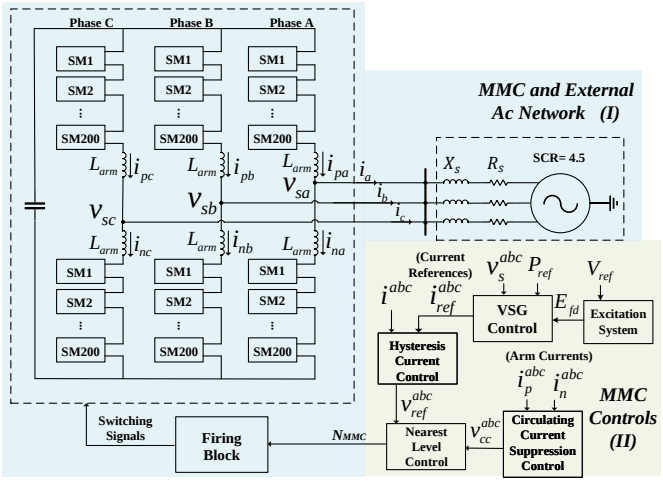

Fig. 3. Overall system layout and control diagram.

TABLE II
MAIN PARAMETERS

Parameter	Value
Number of submodules per arm	200
Dc side voltage	$\pm 150kV$
MMC rated power	$270MW$
Ac system frequency	$60Hz$
Ac system voltage ($l-l, RMS$)	$180kV$
Ac system short circuit ratio (SCR)	4.5
Half of the hysteresis band 'hy'	$0.01pu$

Once the voltages v_{ref}^{abc} are determined by the hysteresis controller, the standard controllers for MMC operation are applied [20]; which include: i) a circulating current suppression controller (CCSC) which is used to cancel circulating current harmonics in the MMCs arms, ii) a capacitor voltage balancing controller for properly adjusting the SMs voltages and iii) a nearest level control (NLC) algorithm for calculating the required number of active submodules in each arm (N_{MMC}). In the end, the firing block generates the necessary firing pulses to turn the appropriate submodules on or off.

V. VALIDATION OF THE OPTIMIZATION USING ELECTROMAGNETIC TRANSIENTS SIMULATION

This section presents two optimization scenarios that have been illustrated and confirmed through EMT simulation. Initially, the optimization focuses on enhancing the damping performance of the VSG by fine-tuning its parameters based on the SS model. It is important to note that this optimization is conducted for a specific operating condition, prompting the need to explore its robustness and evaluate the suitability of the tuned parameters for other operating conditions. Consequently, the subsequent case study demonstrates a robust optimization approach that remains valid across the anticipated operating range. This is achieved by adapting the objective function to account for multiple operating points within the MMC.

A. Optimization for the VSG with Unity Output Power

The optimal parameters of the VSG to solve (18) are obtained using the GA presented in Sec. III, for the VSG operating at the rated power of $P_t = 1.0\ pu$. The hyper-parameters (i.e., parameters of the algorithm as opposed to the parameters being optimized) of the GA were as follows: population size $N = 300$ solutions and maximum number of generations $G = 500$. These hyper-parameters were selected with a modicum of trial and error.

Table III shows the optimal parameters of the VSG after optimization, as well as their percentage variations from the original values (which were chosen as the typical values for a real SG). The optimization results show that although most values change appreciably, the most dramatic change occurs for the virtual resistance, ranging from 226 % to 5023 %. This outcome is in line with expectations, considering that the larger resistance should provide better damping. Note that in a real machine, many of the optimized values would be impractical to achieve, but that is not the case for the virtual machine.

TABLE III
OPTIMIZED PARAMETERS OF VSG FOR $P_t = 1.0\ pu$

Parameter	Original Value	Optimized Value	Percentage Difference
H	$3.42\ s$	$3.0597\ s$	-10.54 %
D_w	5.0	5.2988	5.98 %
R_a	$0.0043\ pu$	$0.04439\ s$	932.33 %
R_{1d}	$0.01823\ pu$	$0.05944\ pu$	226.06 %
R_{fd}	$0.0008947\ pu$	$0.00693\ pu$	672.53 %
R_{1q}	$0.0104\ pu$	$0.53288\ pu$	5023.80 %
L_a	$0.015\ pu$	$0.01545\ pu$	3.00 %
L_{md}	$2.0\ pu$	$2.70179\ pu$	35.09 %
L_{fd}	$0.119\ pu$	$0.02788\ pu$	-76.57 %
L_{1d}	$0.1097\ pu$	$0.07640\ pu$	-30.36 %
L_{mq}	$1.44\ pu$	$1.99778\ pu$	38.73 %
L_{1q}	$0.395\ pu$	$0.05247\ pu$	-86.72 %

Fig. 4 (a) shows the step responses with $\Delta P_{ref} = -0.1\ pu$ of the SS model as well as the EMT simulation with original parameters and Fig. 4 (b) with optimized parameter. Firstly, the EMT and small signal models completely overlap, confirming the accuracy of the small signal model. Secondly, the optimized transient response in (b) is significantly better than the original response in (a) and the damping ratio of the dominant mode increases almost seven-fold from 0.109 to close to $1/\sqrt{2}$. Also, the optimized settling time of $t_s = 0.657\ s$ is much shorter than the settling time of $t_s = 1.699\ s$ with the original parameters. Note that although the small signal model was used in order to speed up the calculation of the fitness function, the full EMT simulations confirm that the results obtained are quite accurate.

As mentioned in section I, other non-liner optimization algorithms capable of dealing with many decision variables could have been used to solve the problem. Table IV shows the result of the optimization when also solving the same problem with PSO and DE. As can be seen, they all find answers with damping factor essentially equal to the desired value of 0.707.

TABLE IV
BEST FITNESS OBTAINED WITH DIFFERENT OPTIMIZATION ALGORITHMS.

	GA	PSO	DE
Best fitness	0.7070	0.7069	0.7070

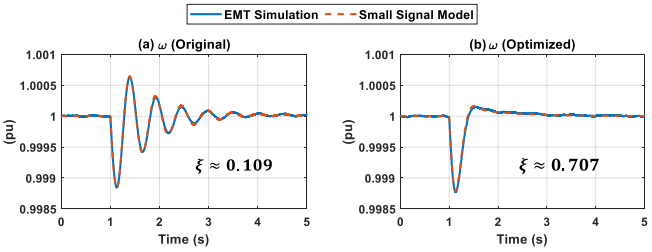

Fig. 4. Virtual rotor speed ω under active power step change with (a) original parameters (b) optimized parameters.

From the above results, it is clear that the VSG's parameters are not restricted to the physical parameter ranges of an actual synchronous generator, and can be chosen freely to give a markedly improved performance. However, the above optimization was carried out for a specific operating point, so the question arises whether the parameters can be selected so that the performance is acceptable over the entire range of power loadings.

Selecting parameters that optimize the performance for $P_t = 1.0\ pu$ gives an excellent damped result (with $\xi = 0.707$) for that operating point. However, as is evident from Fig. 5, the same parameters give a less than desired result for another operating point, e.g., $P_t = 0.1\ pu$, in which case the damping drops to $\xi = 0.139$. To address this issue, the following section presents a robust optimization approach that gives good performance over the entire range.

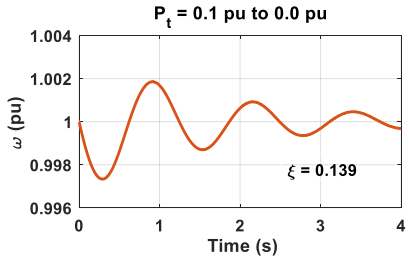

Fig. 5. Virtual rotor speed ω with optimized parameters under avtive power step change in EMT simulation.

B. Optimization for Multiple Operating Points

In order to make the parameter selection robust [17] (i.e., valid over the projected operating range), instead of using the dominant eigenvalue at a single operating point as in (19), a weighted sum of the dominant eigenvalues at each of the M operating points is used as in (21), and depicted in Fig. 6.

In this example, $M = 3$ typical operating points of $P_1 = 0.5\ pu$, $P_2 = 0.7\ pu$, and $P_3 = 1.0\ pu$, are considered. Also, equal weights $W_{1,2,3} = 1/3$, are assumed.

$$\xi_{dom} = \sum_{m=1}^{M} \min \left(\frac{-\sigma_{k,m}}{\sqrt{\sigma_{k,m}^2 + \omega_{k,m}^2}} \right) W_m \qquad (21)$$

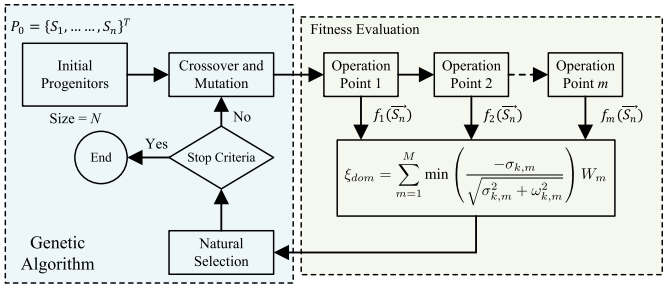

Fig. 6. Modified GA procedure including robustness.

Table V shows the VSG's parameters after the robust optimization which considers multiple operating points. The dominant damping ratios for four different operating points are given in Table VI with these optimized parameters. The damping ratios of VSG with the previous parameter set (in Table III) which was optimized only for the rated condition are also listed for comparison.

It is clear that the VSG with the robust set of parameters gives an overall optimized response over the range of operating points. However, the response for a particular operating point may be sub-optimal. For example, the optimal performance for $P_t = 1.0\ pu$ gives $\xi = 0.707$, but drops marginally to $\xi = 0.532$ when we sacrifice some performance in order to provide universally good damping over the expected operating range.

TABLE V
PARAMETERS OF VSG WITH ***Robust*** OPTIMIZATION INCLUDING MULTIPLE OPERATING POINTS

Parameter	Optimized value	Parameter	Optimized value
H	3.3775 s	L_a	0.00948 pu
D_w	5.0998	L_{md}	1.98853 pu
R_a	0.10502 pu	L_{fd}	0.02473 pu
R_{1d}	0.03396 pu	L_{1d}	0.11581 pu
R_{fd}	0.00785 pu	L_{mq}	1.45503 pu
R_{1q}	0.02917 pu	L_{1q}	0.29485 pu

TABLE VI
DOMINANT DAMPING RATIO OF DIFFERENT OPERATING POINTS

Operating Point (Output Power P_t)	VSG with Optimized Parameters	VSG with Robust Parameters
$P_t = 1.0pu$	0.707	0.532
$P_t = 0.7pu$	0.698	0.571
$P_t = 0.5pu$	0.561	0.538
$P_t = 0.1pu$	0.139	0.416

Fig. 7 shows the step response in the virtual rotor speed ω with a step reduction in output power of 0.1 pu for two operating points ($P_t = 1.0\ pu$ and $P_t = 0.1\ pu$). After the robust optimization that takes into account the expected

operating range, the performance is well damped at both operating points (compare with Figs. 4 (b) and 5).

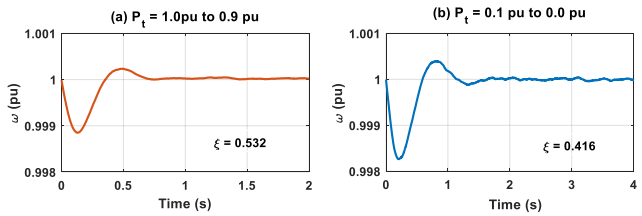

Fig. 7. Virtual rotor speed ω with robustly optimized parameters under active power step change in EMT simulation.

C. Response to a Frequency Change

The performance with the robust optimized parameter set was tested for other disturbances such as a step change in frequency. Fig. 8 illustrates the response of the virtual rotor speed ω (obtained by EMT simulation) with a step change in system frequency from $60.0\ Hz$ to $59.0\ Hz$. The original parameters set (in Table III) and the robust parameters set derived in previous section (in Table V) were used. The results clearly demonstrate that the robust optimized parameters still provide a significant damped lead to a enhanced transient response to the grid frequency disturbance, exhibiting a smaller settling time ($t_s = 0.726\ s$) and a larger damping ratio ($\xi = 0.4348$) compared to the original parameters ($t_s = 1.623\ s$ and $\xi = 0.1229$).

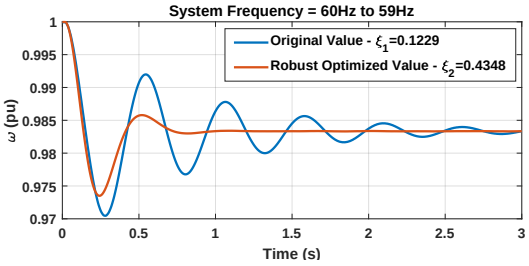

Fig. 8. Virtual rotor speed ω with original parameters and robust optimized parameters under grid frequency step change from $60Hz$ to $59Hz$.

VI. Conclusions

The parameters of the virtual synchronous generator are not confined to any physical range as those for a real synchronous generator are. This paper demonstrates that, removed from the above physical restriction, a Genetic Algorithm can select the parameters of the VSG to significantly improve performance of the system.

Optimization can be carried out for a specific operating point. For example, at rated power, the dominant damping ratio of the test system could attain the idealized value of $\xi = 0.707$, which has a major increase compared with the pre-optimized case ($\xi = 0.109$). It was observed that the damping was most sensitive to the virtual resistances of the windings. The values of the optimized resistances were significantly different, some as much as 50 times larger than the pre-optimized values.

As is clear, optimizing the parameters for a single operating point gave the best performance at that point, but the VSG behaved poorly at other operating points. This was corrected by conducting a robust optimization, where the objective function was modified to be the weighted sum of the objective functions of several individual operating points over the intended operating range. It was shown that doing so gave an universally good performance for the range of intended operating points, although it might prove a trifle sub-optimal for any specific operating point. Also, the system with the optimized parameters exhibits enhanced damping performance with the step change in grid frequency, achieving a damping ratio of $\xi = 0.4328$.

References

[1] J. Arrillaga, *High Voltage Direct Current Transmission*. 2nd Edition. London, 1998.

[2] H. Zhang, W. Xiang, W. Lin, and J. Wen, "Grid forming converters in renewable energy sources dominated power grid: Control strategy, stability, application, and challenges," *Journal of Modern Power Systems and Clean Energy*, vol. 9, no. 6, pp. 1239–1256, 2021.

[3] Q.-C. Zhong and G. Weiss, "Synchronverters: Inverters that mimic synchronous generators," *IEEE Transactions on Industrial Electronics*, vol. 58, no. 4, pp. 1259–1267, 2011.

[4] J. Roldán-Pérez, A. Rodríguez-Cabero, and M. Prodanovic, "Design and analysis of virtual synchronous machines in inductive and resistive weak grids," *IEEE Transactions on Energy Conversion*, vol. 34, no. 4, pp. 1818–1828, 2019.

[5] S. DArco, J. A. Suul, and O. B. Fosso, "A virtual synchronous machine implementation for distributed control of power converters in smartgrids," *Electric Power Systems Research*, vol. 122, pp. 180–197, 2015.

[6] P. Rodríguez, C. Citro, J. I. Candela, J. Rocabert, and A. Luna, "Flexible grid connection and islanding of spc-based pv power converters," *IEEE Transactions on Industry Applications*, vol. 54, no. 3, pp. 2690–2702, 2018.

[7] A. F. Darbandi, A. Sinkar, and A. Gole, "Effect of short-circuit ratio and current limiting on the stability of a virtual synchronous machine type gridforming converter," in *The 17th International Conference on AC and DC Power Transmission (ACDC 2021)*, vol. 2021, 2021, pp. 182–187.

[8] C. Jiang, A. D. Sinkar, and A. M. Gole, "Comparative study of swing equation-based and full emulation-based virtual synchronous generators," in *11th International Conference on Power Electronics, Machines and Drives (PEMD 2022)*, vol. 2022, 2022, pp. 578–582.

[9] C. Jiang, "Advanced virtual synchronous generator implementation on a modular multilevel converter," Ph.D. dissertation, University of Manitoba, 2023.

[10] C. Jiang, A. D. Sinkar, and A. M. Gole, "Small signal analysis of a grid-forming modular multilevel converter with a novel virtual synchronous generator control," *Electric Power Systems Research*, vol. 223, p. 109621, 2023.

[11] K. Ogata, *Modern Control Engineering*, ser. Instrumentation and controls series. Prentice Hall, 2010.

[12] K. Y. Lee and M. A. El-Sharkawi, Eds., *Modern Heuristic Optimization Techniques*. Hoboken, NJ, USA: John Wiley & Sons, Inc., Jan 2008.

[13] J. Del Ser, E. Osaba, D. Molina, X. S. Yang, S. Salcedo-Sanz, D. Camacho, S. Das, P. N. Suganthan, C. A. Coello Coello, and F. Herrera, "Bio-inspired computation: Where we stand and what's next," *Swarm and Evolutionary Computation*, vol. 48, no. December 2018, pp. 220–250, 2019.

[14] P. A. Vikhar, "Evolutionary algorithms: A critical review and its future prospects," *Proc. - Int. Conf. Glob. Trends Signal Process. Inf. Comput. Commun. ICGTSPICC 2016*, vol. -, pp. 261–265, 2017.

[15] F. Gerges, G. Zouein, and D. Azar, "Genetic algorithms with local optima handling to solve sudoku puzzles," in *Proceedings of the 2018 International Conference on Computing and Artificial Intelligence*, ser. ICCAI 2018. New York, NY, USA: Association for Computing Machinery, 2018, p. 1922.

[16] L. M. Schmitt, "Theory of genetic algorithms ii: models for genetic operators over the string-tensor representation of populations and convergence to global optima for arbitrary fitness function under scaling," *Theoretical Computer Science*, vol. 310, no. 1, pp. 181–231, 2004.

[17] A. Gole, S. Filizadeh, and P. Wilson, "Inclusion of robustness into design using optimization-enbaled transient simulation," *2005 IEEE Power Engineering Society General Meeting*, vol. 2, no. 3, p. 1125, 2005.

[18] P. Kundur, N. Balu, and M. Lauby, *Power System Stability and Control*, ser. EPRI power system engineering series. McGraw-Hill Education, 1994.

[19] H. T. Tuan, "Stability of fractional-order nonlinear systems by lyapunov direct method," *IET Control Theory & Applications*, vol. 12, pp. 2417–2422(5), November 2018.

[20] K. Sharifabadi, L. Harnefors, H.-P. Nee, S. Norrga, and R. Teodorescu, *Design, Control, and Application of Modular Multilevel Converters for HVDC Transmission Systems*. John Wiley and Sons, 2016, pp. 7–59.